PUBLICATIONS OF THE ASTRONOMICAL SOCIETY OF THE PACIFIC, **124**:586–597, 2012 June

Design and Construction of Absorption Cells for Precision Radial Velocities in the *K* Band Using Methane Isotopologues

GUILLEM ANGLADA-ESCUDÉ,[1] PETER PLAVCHAN,[2] SEAN MILLS,[3] PETER GAO,[3] EDGARDO GARCÍA-BERRÍOS,[4] NATHAN S. LEWIS,[4] KEEYOON SUNG,[5] DAVID CIARDI,[2] CHAS BEICHMAN,[2] CAROLYN BRINKWORTH,[2] JOHN JOHNSON,[3] CASSY DAVISON,[6] RUSSEL WHITE,[6] AND LISA PRATO[7]

Received 2011 August 18; accepted 2012 April 24; published 2012 May 22

ABSTRACT. We present a method to optimize absorption cells for precise wavelength calibration in the near-infrared. We apply it to design and optimize methane isotopologue cells for precision radial velocity measurements in the K band. We also describe the construction and installation of two such cells for the CSHELL spectrograph at NASA's IRTF. We have obtained their high-resolution laboratory spectra, which we can then use in precision radial velocity measurements and which can also have other applications. In terms of obtainable RV precision, methane should outperform other proposed cells, such as the ammonia cell ($^{14}NH_3$) recently demonstrated on CRIRES/VLT. The laboratory spectra of the ammonia and methane cells show strong absorption features in the H band that could also be exploited for precision Doppler measurements. We present spectra and preliminary radial velocity measurements obtained during our first-light run. These initial results show that a precision down to 20–30 m s^{-1} can be obtained using a wavelength interval of only 5 nm in the K band and S/N $\sim$ 150. This supports the prediction that a precision down to a few meters per second can be achieved on late-M dwarfs using the new generation of NIR spectrographs, thus enabling the detection of terrestrial planets in their habitable zones. Doppler measurements in the NIR can also be used to mitigate the radial velocity jitter due to stellar activity, enabling more efficient surveys on young active stars.

Online material: color figures

1. INTRODUCTION

The radial velocity (RV) technique is the most efficient method to detect planetary-mass bodies orbiting stars. Accuracies at the level of $\sim$1 m s^{-1} have been recently achieved with state-of-the-art optical spectrographs such as HARPS/ESO (Mayor et al. 2009), HIRES/Keck (Howard et al. 2010), or PFS/Magellan (Crane et al. 2010). The radial velocity technique is most sensitive to massive planets around low-mass stars, but such stars are intrinsically faint at optical wavelengths, and only a handful of nearby and relatively massive M dwarfs have been successfully monitored for planetary systems (e.g., Endl et al. 2006; Johnson et al. 2007; Zechmeister et al. 2009). Although the number of M dwarfs surveyed in the optical is small, they have produced some of the most spectacular results in the field: multiplanetary systems with several super-Earths (GJ 581; Mayor et al. 2009; Vogt et al. 2010), the first transiting Neptune-mass planets (GJ 436 and GJ 1214; Gillon et al. 2007; Charbonneau et al. 2009), and the most dynamically complex systems with both giant planets and super-Earth–mass bodies (GJ 876bcde; Rivera et al. 2010). Thus, there is strong statistical evidence that M dwarfs are rich in sub–Neptune-mass planets (Mayor et al. 2009) and (possibly) Earth-mass planets as well (Howard et al. 2010).

Since most of the flux of M dwarfs is emitted in the near-infrared (NIR), many more and later-type M dwarfs could be surveyed, provided that adequate wavelength-calibration techniques and spectrographs are developed in the NIR region (e.g., Reiners et al. 2010). Additionally, young and/or active stars will have relatively more quiescent photospheres in the NIR relative to the optical, allowing for wavelength-dependent characterization or mitigation of stellar jitter (Bailey et al. 2011).

Recently, Bean et al. (2010b) have shown that accuracy at the $\sim$5–10 m s^{-1} level can be achieved on timescales of several months using an absorption cell filled with ammonia gas ($^{14}NH_3$). This ammonia cell has been used to rule out the presence of the astrometric planet candidate around the low-mass

[1] Carnegie Institution of Washington, Department of Terrestrial Magnetism, 5241 Broad Branch Road NW, Washington DC, 20015, anglada@dtm.ciw.edu.
[2] NASA Exoplanet Science Institute, 770 South Wilson Avenue, Mail Code 100-22, Pasadena, CA 91125, plavchan@ipac.caltech.edu.
[3] Department of Astronomy, California Institute of Technology, 1200 East California Boulevard, Mail Code 249-17, Pasadena CA 91125.
[4] Division of Chemistry and Chemical Engineering, California Institute of Technology, 210 Noyes Laboratory, Mail Code 127-72, Pasadena, CA 91125.
[5] Jet Propulsion Laboratory, California Institute of Technology, 4800 Oak Grove Drive, Pasadena, CA 91109.
[6] Georgia State University, Department of Physics and Astronomy, 29 Peachtree Center Avenue, Science Annex, Suite 400, Atlanta, GA 30303.
[7] Lowell Observatory, 1400 West Mars Hill Road. Flagstaff, AZ 86001.

M8.5V star VB10 (Bean et al. 2010a). Fostered by the success of this pioneering technique, we started a collaboration to design, build, and implement optimized absorption cells on the available (and near-future) NIR spectrographs.

During our investigation, we found that methane is, in fact, a very suitable gas for wavelength calibration in the K band. The frequency precision and accuracy of CH_4 achieved by Boudon et al. (2009)[8] indicates that methane absorption features can be good enough for RV observations. The viability of $^{12}CH_4$ as a wavelength standard at other wavelengths is well proven. We refer the reader to the Bureau International des Poids et Mesures,[9] or Shen et al. (1981) for examples detailing the use of methane as a wavelength-calibration standard in other lines of inquiry. Despite this, it is well known to astronomers working in the near-infrared domain (1.0 to 5 μm) that the Earth's atmosphere contains sufficient methane to also produce deep absorption features, especially beyond 2.0 μm. Therefore, it would be difficult to accurately disentangle these telluric absorption features from those created by a cell containing standard $^{12}CH_4$. However, carbon and hydrogen have other stable isotopes that also form chemically stable isotopologues of methane. The substitution of an atom by another isotope significantly shifts the absorption features of a molecule. As shown later, we find that such a shift is large enough to avoid confusion of the methane isotopologues with the more common $^{12}CH_4$. The preliminary design of optimal gas cells is done using the line lists available in the HITRAN 2008 database (Rothman et al. 2009). We concentrate this study on the two simpler methane isotopologues $^{13}CH_4$ (methane-13) and $^{12}CH_3D$ (deuterated methane) and compare their performance to ammonia ($^{14}NH_3$). Since we have built a cell for each gas, we also provide the construction details for such cells.

The $^{13}CH_4$ cell has been installed and used in a prototype program on the CSHELL spectrograph at NASA's Infrared Telescope Facility (IRTF). We present the first-light spectra of bright stars through this cell, illustrating that the proposed setup is ready to begin precision RV measurements. The use of the cell and the Fourier-transformed infrared (FTIR) spectra are available to the community.

2. OPTIMIZING A GAS CELL FOR A SPECTROGRAPH

2.1. Free Parameters

When using a gas absorption cell for precise wavelength calibration, its transmission absorption spectrum will determine the maximum achievable RV precision. The cell absorption spectra mainly depend on the following parameters: length of the cell, gas used, gas temperature, gas pressure, and spectral resolution set by the spectrograph. Among these parameters, the only relevant freedom is the choice of the gas and its pressure. For practical reasons, the cell temperature should be around 300 K. A few tens of kelvins do not make a substantial difference in the absorption spectra of the gases under consideration. Longer optical paths produce deeper and sharper features, which are both desirable to obtain a better wavelength-calibration setup. Therefore, the cell length should be as long as is physically allowed by the spectrograph (e.g., ~20 cm; Bean et al. 2010b). A cell with multiple reflections could be used to increase the optical depth at the cost of a more bulky setup and some losses in each reflection (see Mahadevan & Ge [2009] as an example). We will not discuss this option here.

The spectral resolution is a measure of the smallest separation $\delta\lambda$ at which spectral features can be distinguished. In astronomical spectrographs, it is usually defined in relation to the resolving power $R = \lambda/\delta\lambda$, which is ideally constant with wavelength. To obtain the maximal RV precision, $\delta\lambda$ needs to be as small as possible or, equivalently, R has to be as large as possible. The stellar spectral features have to be resolved when using traditional spectroscopy to measure precise RVs (as opposed to externally dispersed interferometers; see Ge et al. [2002] as an example). The range of available spectral resolution for precise RV measurements is around $R \sim 30,000$ (e.g., NIRSPEC/Keck; McLean et al. 1998) to $R = 110,000$ (CRIRES/VLT; Kaeufl et al. 2004). As an example, $R \sim 30,000$ implies that at 2300 nm one can resolve a $\delta\lambda$ of 0.076 nm, while 0.0209 nm can be resolved if $R = 110,000$. As shown later, the resolution of the spectrograph is a critical element in the choice of the right gas and pressure. As a general rule, $\delta\lambda$ is defined as the full width at half-maximum (FWHM) of the point-spread function (PSF) in the wavelength-dispersion direction. This PSF (also called instrumental profile) is intrinsic to each instrument and has nothing to do with the physical processes involved in the generation of absorption lines in the intervening gas or the stellar spectrum. For simulation purposes, the shape of this instrumental profile can be approximated by a Gaussian profile or an ensemble of Gaussian profiles. The precise shape will only be relevant in the actual reduction of the observations and will be different for each instrument. Strictly speaking, a Gaussian profile has a $\sigma = \mathrm{FWHM}/2.35$; however, typical instrumental line-spread functions (LSFs) tend to have higher wings, effectively degrading the actual resolution. For the purpose of quantifying the dependence of the maximum precision as a function of the spectral resolution, we assume that the instrumental profile is a Gaussian with $\sigma = \delta\lambda/2$. The product of the stellar spectrum, the absorption spectrum of the gas cell, and the absorption of the atmosphere have to be convolved with this instrumental profile to obtain the observed (simulated) spectrum.

In summary, given room-temperature operating conditions of ~300 K, a cell length of the order of ~10 cm, and an optimal spectral resolution (depends on the spectrograph design details), the gas pressure is the only free parameter to adjust to reach the maximal RV precision.

[8] Methane on Titan project, maintained by Vincent Boudon, http://www.icb.cnrs.fr/titan/.

[9] See http://www.bipm.org/en/publications/mep.html.

2.2. Choice of Gases and Optimization Metric

In the preliminary phase of our investigation, we were interested in assessing which gas was more adequate for RV measurements in the K band. To quantitatively compare the nominal performance of a gas cell paired with a spectrograph, we used the photon-noise-limited precision σ_V as derived by Butler et al. (1996) as our metric. The photon-noise-limited precision has two components: the contribution of the gas cell σ_c and the contribution of the stellar spectrum σ_*. The contribution of the gas cell σ_c represents how well the wavelength of each pixel can be measured, while σ_* represents how well a stellar Doppler offset can be measured given the richness of spectral features on the stellar spectrum. The expression for σ_V reads

$$\sigma_V = \sqrt{\sigma_c^2 + \sigma_*^2}, \tag{1}$$

$$\sigma_c = c\left(\sum_{\text{pixels}} \lambda \frac{dI_c}{d\lambda} \times \text{S/N}\right)^{-1/2}, \tag{2}$$

$$\sigma_* = c\left(\sum_{\text{pixels}} \lambda \frac{dI_*}{d\lambda} \times \text{S/N}\right)^{-1/2}. \tag{3}$$

where c, when not a subscript, is the speed of light; I is the intensity of the stellar spectrum ($*$) or the cell (c) spectra normalized to a continuum equal to 1; λ is the wavelength in meters; and S/N is the signal-to-noise ratio at each element of the sum and is equal to $(N_{\text{phot}})^{1/2}$ assuming Poisson statistics. The sum is calculated over all the resolution elements $\delta\lambda$. Modern spectrographs are usually designed in such a way that each $\delta\lambda$ is covered by two or more sampling elements (or pixels). As long as there is more than one pixel on each $\delta\lambda$, the number of pixels used does not affect the nominal photon-noise limit. For example, let us assume a S/N of 100 on each $\delta\lambda$ ($N_{\text{phot}} = 10,000$). If we have 2 pixels on each $\delta\lambda$, each pixel will collect 5000 photons and a corresponding S/N per pixel of 70.7. However, the loss of S/N per pixel is compensated in equation (1) by having twice the number of elements in the sum. In reality, a larger number of pixels (e.g., >2) per $\delta\lambda$ is always better to model the instrumental profile. The sampling of the profile will contribute to the final error budget, irrespective of the chosen calibration gas; therefore, in a relative sense, it does not affect our comparison metric.

The photon-noise-limited precision σ_V is the function to be minimized with respect to the gas parameters (as we discussed, only pressure). Note that this is an ideal estimate of the final RV precision. The real observations will contains additional sources of uncertainty, such as the detector performance, instrumental profile modeling, availability of adequate stellar templates, and contamination by telluric features. At this time, the major limitation to achieve high precision is the limited number of high-resolution spectrographs with near-infrared capabilities and the limited wavelength range they can provide in each single exposure. The only instrument able to deliver spectral resolution over 10^5 is CRIRES/VLT, and it is still a single-order spectrograph covering only 40 nm at 2.3 μm (Bean et al. 2010b). The quality and size of the NIR imaging arrays is also a limiting factor on some instruments, such as NIRSPEC/Keck (Bailey et al. 2011), which is also limited by a relatively low resolution $R \sim 30,000$. It is expected that new NIR spectrographs will have a significantly increased spectral grasp and will incorporate newly developed high-quality CMOS imaging arrays,[10] greatly mitigating the systematic uncertainties due to the detector performance on fainter targets.

2.3. Methane Versus Ammonia

The two gases we compare here are ammonia and methane. Yurchenko et al. (2005) and Huang et al. (2008) predicted that the NIR spectral features of ammonia were useful as a frequency-calibration source for RV observations (see also Urban et al. 1989). A cell with the most common isotopologue of ammonia (hereafter, $^{14}NH_3$) has already been demonstrated at the telescope (Bean et al. 2010b, 2010a), so we wanted to assess if it was worth developing a brand new cell based on an alternative gas (methane). Both gases have good-quality line lists in the HITRAN 2008 database (Rothman et al. 2009; beyond 1.9 μm for ammonia and from 1.0 to >5 μm for methane), allowing straightforward simulations of the spectra for a given set of cell parameters. Ammonia also has abundant spectral features below 1.6 μm, and they have been recently reported by Sung et al. (2012, in preparation), but at the time we built our cells, those lines were unknown to us and we do not discuss them in detail here. Some alternative gases for work in the H band have been given by Valdivielso et al. (2010) and Mahadevan & Ge (2009). The method of cell optimization presented herein can be applied to any other gas given the required information to generate synthetic absorption spectra (line lists or public FTIR spectra). As a matter of fact, a simplified version of the analysis presented here was done on most of the gases available in the HITRAN 2008 database. Methane was identified as a promising gas during such quick-look analysis.

As discussed before, it is well known that telluric methane features are omnipresent in NIR spectra (especially in the K and redder bands). In order to avoid blends of the calibration spectrum with telluric features, we propose using methane isotopologues instead ($^{13}CH_4$ and $^{12}CH_3D$). At the obtained working pressures and temperatures, they are both easy to handle and much less reactive than $^{14}NH_3$. It also helps that enough gas to build several cells could be purchased for a few hundred dollars. The NIR absorption features of methane are molecular rotovibrational transitions related to the C-H bond and the moment of inertia of the methane molecule. The main difference between

[10] See, e.g., http://www.teledyne-si.com/infrared_sensors/index.html.

$^{12}CH_4$ and $^{13}CH_4$ is a change in the reduced mass of the ^{13}C-H bond, changing the wavelengths of the $^{12}CH_4$ transitions by a multiplicative factor. In the case of $^{12}CH_3D$, the substitution of a C-H by a C-D bond adds an additional oscillator and breaks the tetrahedric symmetry of the molecule. As a result, the $^{12}CH_3D$ spectrum is a *scrambled* version of $^{12}CH_4$. Even though there is extensive literature on the interpretation of the absorption spectrum for both isotopologues, no comprehensive line lists are readily available in a straightforward format. The HITRAN 2008 database contains some lines of all three methane isotopologues in a narrow range between 3.0 and 3.5 μm (see Fig. 1). Using the centers of the sharper lines between 3.0 and 3.5 μm, we find that a multiplicative factor of ~1.0032 is needed to reproduce the wavelength shift in the lines of $^{13}CH_4$ with respect to $^{12}CH_4$. This number is an simplification of the complex rovibrational spectral transition changes between the two isotopes. However, this multiplicative factor approximation enables one to obtain a realistic spectrum of $^{13}CH_4$ in terms of the approximate line density and depth as a function of wavelength and to consequently evaluate the performance of $^{13}CH_4$ as a wavelength-calibration gas. At the K band ($\lambda \sim 2300$ nm), this will translate into a shift of ~8 nm with respect the equivalent features in $^{12}CH_4$. More importantly, this shift is more than sufficient to avoid blends with telluric $^{12}CH_4$ features (typical width of 0.1 nm at the K band; see § 4.2). Figure 1 also illustrates that the spectrum of $^{12}CH_3D$ is a scrambled version of $^{12}CH_4$, but with shallower features.

In overview, the absorption spectra of $^{14}NH_3$ and $^{12}CH_4$ can be simulated to a high degree of realism by using the line lists available in the HITRAN 2008 database and a basic ray-tracing software. Concerning the ray-tracing software, we explored several options and found that the Reference Forward Model package[11] provided the most straightforward and simplest approach to obtain the desired synthetic spectra. We compared our simulated spectra with those computed with SpectralCalc[12], obtaining perfect agreement among the two. As discussed before, the absorption spectra of $^{13}CH_4$ is obtained to the required level of realism by applying a multiplicative factor to the wavelengths of the $^{12}CH_4$ spectrum. As will be shown in § 4.2, this approach worked very well in the estimation of the optimal pressure for the $^{13}CH_4$ cell. Because the absorption spectrum of $^{12}CH_3D$ is very different from $^{12}CH_4$, we could not perform the same optimization analysis. Since the $^{12}CH_3D$ lines at 3.5 μm are shallower than those from $^{12}CH_4$, we tentatively built it with a pressure slightly higher than the optimal one found for the $^{13}CH_4$ cell. As shown later, such pressure turned to be insufficient to produce deep-enough lines. Now that the spectrum of $^{12}CH_3D$ is known, we will be able to use it to optimize future cells. Hereafter, all the optimization details refer only to $^{14}NH_3$ and $^{13}CH_4$.

[11] Reference-forward model, maintained by Anu Dudhia, http://www.atm.ox.ac.uk/RFM/.

[12] Available at http://www.spectralcalc.com/.

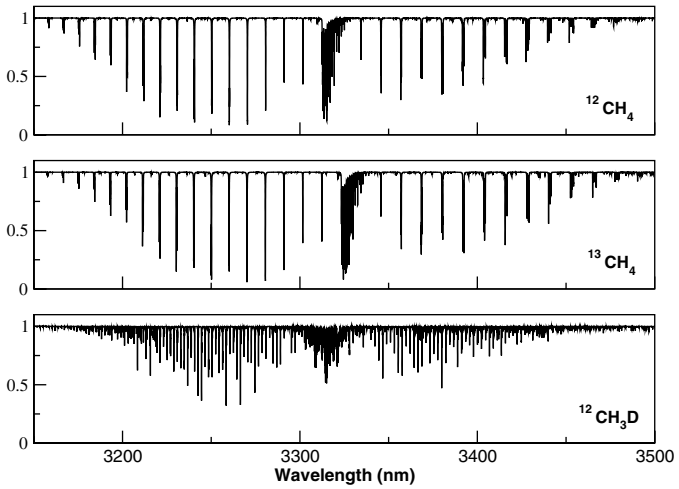

FIG. 1.—Synthetic absorption at 3.0 μm of the three isotopologues of methane available at the HITRAN 2008 database. Methane is a very strong absorber at this wavelength, so cell lengths of a few millimeters or centimeters have been used to generate this example spectra ($T = 300$ K, $P = 300$ mbar).

2.4. Model Configuration Setup

For the purposes of our optimization models, the length of all the cells is fixed at 10 cm. We also assume an ideal spectrograph continuously covering an interval of 200 nm at the K band. While an instrument with such capabilities does not yet exist, a comparable wavelength coverage should be within the reach of the proposed NIR spectrographs (e.g., i-Shell on NASA's IRTF and upgraded versions of NIRSPEC/Keck and CRIRES/VLT). Such a wavelength range is also representative of the interval where the cells under discussion (ammonia and methane) show more absorption features in the K band. Note that the cells only provide good wavelength calibration on the spectral region well covered by them, so using the full K band to estimate the performance of each cell would seriously underestimate the stellar contribution to the error budget. The central wavelength of the interval is also obtained during the optimization process. Four spectral resolutions are also tested: 30,000, 50,000, 70,000, and 10^5. These resolutions roughly match the range of available (or planned) NIR spectrographs. To make a fair comparison, we will assume that the number of collected photons is the same in all the setups. In other words, when the resolution is higher, the signal will be spread over a larger number of resolution elements; therefore, the S/N per resolution element will be reduced. The resulting σ_V for various setups and gas cell configurations are given in Figure 2. In addition to the cell parameters, the central wavelength λ_c of the 200 nm window is also optimized. The atmospheric K-band window is surrounded by strong and very variable water absorption features that we want to avoid as much as possible. Neither gas shows enough absorption features below 2100 nm to be useful for wavelength calibration. As a result, the useful wavelength range we test is between 2100 and 2450 nm. For the stellar spectra, we

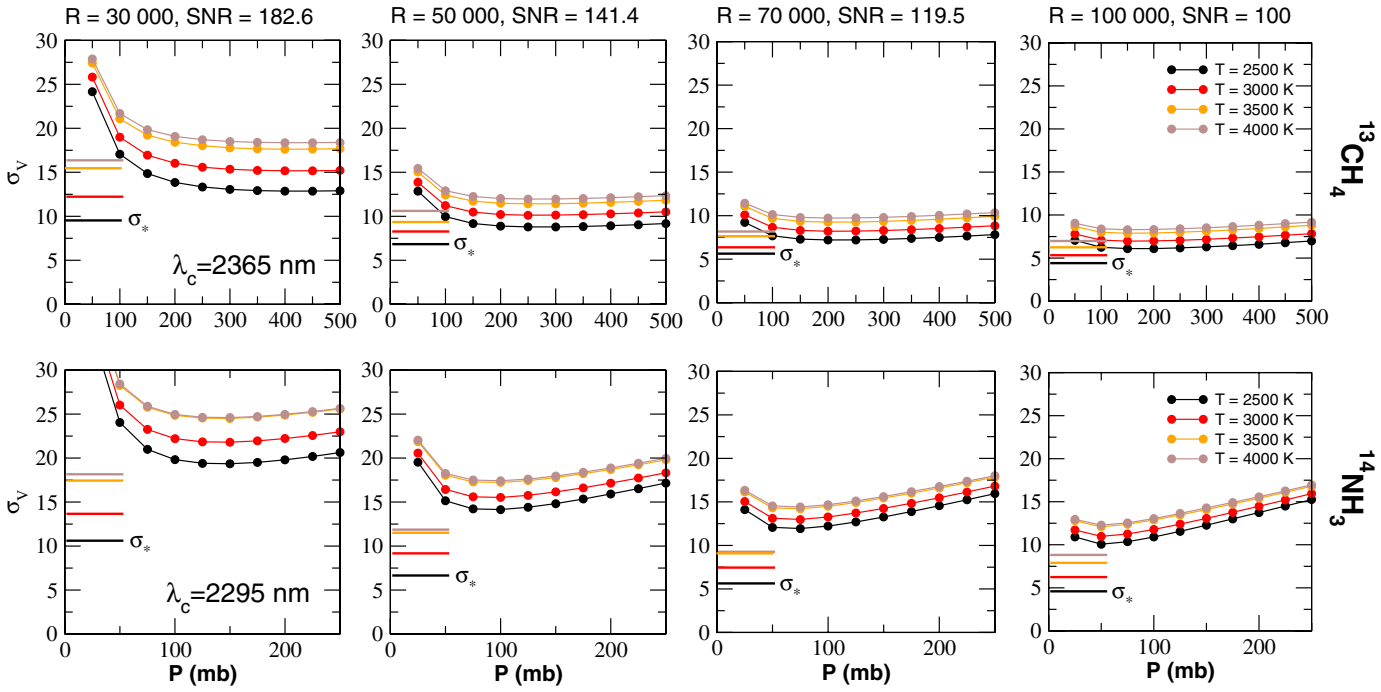

FIG. 2.—Photon-noise radial velocity precision σ_V as a function of gas cell pressure for different stellar atmosphere models (*dots*). Because the spectra of stars depends on the effective temperature, σ_V will also depend on that. *Top*: Results for the $^{13}CH_4$ cell. *Bottom*: Results for $^{14}NH_3$. The contribution of the stellar spectra (*small horizontal lines on the bottom left of each plot*) are also illustrated. Note that the stellar contribution is different for each cell. Because the cells have a higher density of lines on slightly different wavelength ranges, the optimal central wavelength is different for each cell. Such optimal wavelength also weakly depends on the resolution and the gas pressure. The average values of the optimal wavelengths are also given for each setup. In all the cases, $^{13}CH_4$ nominally outperforms $^{14}NH_3$. See the electronic edition of the *PASP* for a color version of this figure.

have used those provided by the PHOENIX[13] group (Hauschildt et al. 1999). Solar metallicity and $\log g = 5.0$ have been assumed in all cases.

3. MODEL RESULTS

For $^{14}NH_3$, σ_V is computed on pressures ranging from 25 to 250 mbar in steps of 25 mbar. For $^{13}CH_4$, the tested pressures go from 50 to 500 mbar in steps of 50 mbar. Figure 2 and Table 1 summarize our results as follows:

1. The optimal gas pressure depends on the spectral resolution. When the pressure is too low, the gas column density is also low and the lines are shallower. When the pressure is high, the lines are deeper due to the increased column density, but they get broader due to pressure-broadening effects. The optimal gas pressures for the proposed setups are given in Table 1.

2. Even accounting for the reduction in the S/N per resolution element, the higher spectral resolution R always provides higher RV precision. The spectrum of the star and the cell are sufficiently resolved at $R = 100,000$, so higher resolutions do not provide a significant improvement (Mahadevan & Ge 2009). Note that we are not discussing the slit size required to achieve each resolution. If a fraction of light L is lost due to bad seeing ($>1.0''$) and/or narrow slit (e.g., $0.2''$), σ_V has to be divided by $\sqrt{L}$. The photon-collection efficiency (also called *throughput*) for a given mode heavily depends on engineering details of each spectrograph (slit size, use of an image slicer, adaptive optics, etc.). The loss of throughput can easily counter the gain in precision from the higher spectral resolution. Therefore, one should first compare the relative performance of the available modes before building a cell optimized for the highest spectral resolution available. As a general approach, we suggest first determining the desired R using synthetic stellar spectra and all the information available on the available observing modes. Only then one should proceed to the gas cell optimization for a given R.

3. Both the stellar and the cell spectra contribute significantly to σ_V. In the case of $^{14}NH_3$, the absorption cell dominates σ_V. As a consequence, the RV measurements will be calibration-noise-limited. On the other hand, the contribution of $^{13}CH_4$ to the overall precision is always smaller than the stellar contribution, which makes it more attractive than $^{14}NH_3$.

4. $^{14}NH_3$ and $^{13}CH_4$ cover a different range of wavelengths. Therefore, the optimal central wavelength λ_c strongly depends on the gas used. To a much lower degree, λ_c also depends on the spectral resolution and pressure; therefore, the optimal

[13] For more information, see http://www.hs.uni-hamburg.de/EN/For/ThA/phoenix/index.html.

TABLE 1

OPTIMAL SETUP FOR VARIOUS TEST SETUPS

Spectral resolution	S/N $(\delta\lambda\eta)^{-1}$	$N_{\delta\lambda}$	λ_c (nm)	$\sigma_{\rm cell}$ ($\rm m\,s^{-1}$)	σ_* ($\rm m\,s^{-1}$)	σ_V ($\rm m\,s^{-1}$)	Pressure (mbar)
			$^{13}CH_4$				
30,000	182	2370	2370	8.9	12.3	15.1	400
50,000	141	4300	2360	6.5	8.0	10.4	300
70,000	119	6021	2360	4.8	6.6	8.2	200
100,000	100	8602	2362	3.8	5.7	6.9	150
			$^{14}NH_3$				
30,000	182	2370	2298	16.7	14.0	21.8	150
50,000	141	4300	2292	12.4	9.3	15.5	100
70,000	119	6021	2298	10.6	7.4	12.9	75
100,000	100	8602	2298	8.7	6.5	10.9	50

NOTE.—We use a stellar atmosphere model for a $T = 3000$ K star and a cell length of 10 cm.

wavelength is always within 5 nm to the values given in Figure 2. Also, $^{13}CH_4$ covers the stellar CO absorption bands better than $^{14}NH_3$, minimizing σ_* and therefore further improving the maximum achievable precision.

The latter two items justify the effort of developing a methane-based absorption cell for future high-precision RV measurements in the NIR. As we mentioned before, each resolution element should contain (at least) 2 pixels or more to properly sample the instrumental profile. If the same S/N can be achieved per pixel instead, then the maximum RV precisions σ_V listed in Table 1 have to be divided by the square root of the number of pixels per resolution element. That is, with the best setup we tested ($R = 100,000$, $^{13}CH_4$, $\sigma_V = 6.9\ \rm m\,s^{-1}$), a star with $T = 3000$ K and 2 pixels per resolution element with a $\rm S/N = 100$ per pixel, one should be able to achieve RV precisions better than $5\ \rm m\ s^{-1}$.

4. OPTIMAL ABSORPTION CELLS FOR IRTF/CSHELL

We started a pilot program to test the absorption cells at the CSHELL spectrograph installed at the NASA/IRTF telescope (Mauna Kea, Hawaii; Tokunaga et al. 1990; Greene et al. 1993). The design parameters and the optimal setup found for this spectrograph are given in Table 2. In addition to testing their performance, we were also interested in the practical issues involved in the construction, installation, and operation of such cells. With this in mind, we built two methane-based cells containing $^{13}CH_4$ and $^{12}CH_3D$, as well as a $^{14}NH_3$ cell for comparison. The construction details and the final high-resolution FTIR spectra of the final cells are given in § 4.2. For this experiment, the central wavelength was not optimized. To simplify the analysis required to obtain precise RV measurements, we chose $\lambda_c = 2312.5$ nm, which is centered in a small window that is relatively free of telluric methane features (see § 4.2).

4.1. Construction of the Cells

Here, we summarize the practical details involved in the construction of the three cells filled with $^{13}CH_4$, $^{12}CH_3D$, and $^{14}NH_3$. In all cases, the construction of the cells is very affordable.

Based on the limitations imposed by the existing extra space in CSHELL, the bodies of the cells were made using a Pyrex tube (12.5 cm in length and 5.1 cm in diameter). Both ends of this tube were capped with low-OH quartz windows with excellent transmission in the NIR. The windows were then coated on the outside with an infrared antireflective coating to further improve transmission. We did not coat the inside of the windows, due to potential chemical reactions of the gas with the coating degrading throughput. Using the laboratory FTIR spectra of all the cells, we found that the overall transmission on the continuum (including the gases) is typically above 80%. Each window is a wedge with an angle of 1.6° oriented 180° relative to the other window on the cell, corresponding to a 2 mm rise in

TABLE 2

DESIGN PARAMETERS AND OPTIMAL SETUP FOR IRTF/CSHELL

Parameter	Value
Spectral resolution	46,000
Cell length	12.5 cm
Cell temperature	283 K
Wavelength interval at K band	~5 nm
$N_{\rm pix}$	256
Optimal $^{13}CH_4$ pressure	275 mbar
Optimal $^{14}NH_3$ pressure	70 mbar
Selected λ_c	2312.5 nm
σ_V ($\rm S/N = 100\ (\delta\lambda)^{-1}$)	~50 m s^{-1}
σ_V ($\rm S/N = 100\ pixel^{-1}$)	~35 m s^{-1}

NOTE.—The stellar model used in the optimization process has $T = 3500$ K, $\log g = 4.5$, and solar metallicity.

window thickness over 7 cm, with a minimum window thickness at one end of 1 mm. This prevents ghost images from appearing on the stellar spectra, which arise from multiple reflections off the spectrograph's optics. The windows were sealed using Varian Torr Seal, a sealant specifically designed to connect glass and maintain a vacuum for a duration longer than a decade in nominal conditions.

Pure anhydrous $^{14}NH_3$ ammonia was purchased from Matheson Tri-Gas (>99.9% quoted purity). The $^{13}CH_4$ isotopologue was purchased from Sigma-Aldrich (99% quoted purity). The more exotic $^{12}CH_3D$ isotopologue was obtained from Cambridge Isotope Laboratories, Inc. (98% quoted purity). All three cells were evacuated using a standard vacuum pump and then filled with the gases. As shown in Table 2, $^{14}NH_3$ and $^{13}CH_4$ cells were found to operate optimally at ~75 mbar and 275 mbar respectively (as a reference, 1013.25 mbar is 1 atm or 1.013^5 Pa). Since we had no means to predict the optimal pressure for $^{12}CH_3D$ at the K band, we filled the $^{12}CH_3D$ cell at a higher pressure (~345 mbar), waiting for the FTIR spectra to evaluate if the cell would be suitable for use at CSHELL. The cells were filled at such pressures at 20°C by means of a small inlet in the side of the Pyrex tube. In order to seal this inlet, the gases were then condensed to a liquid via immersion in an ice bath. This allowed the Pyrex inlet to be heated to ~1100 K without raising the interior gas temperature and pressure. If the gases had been left in the gas phase at 20°C, the internal pressure would have exceeded 1 atm and the gas would have burst out of the hot malleable inlet. The first tests filling our gas cells with ammonia gas resulted in this outcome. The end result of the sealing process allowed for the creation of an essentially permanent Pyrex seal to the inlet, such that the main body tube is a single piece of Pyrex.

All three cells are interchangeable and can easily be substituted as needed by removing the current cell and placing one of the others in the mount. The active cell is mounted inside a calibration box with an aluminum housing, which in turn sits in front of the CSHELL spectrograph entrance window. The gas cell tube is attached to a rotary stage by aluminum braces, which allows the cell to be moved in and out of the telescope's beam by remote operation (see Fig. 3). The remote operation is an

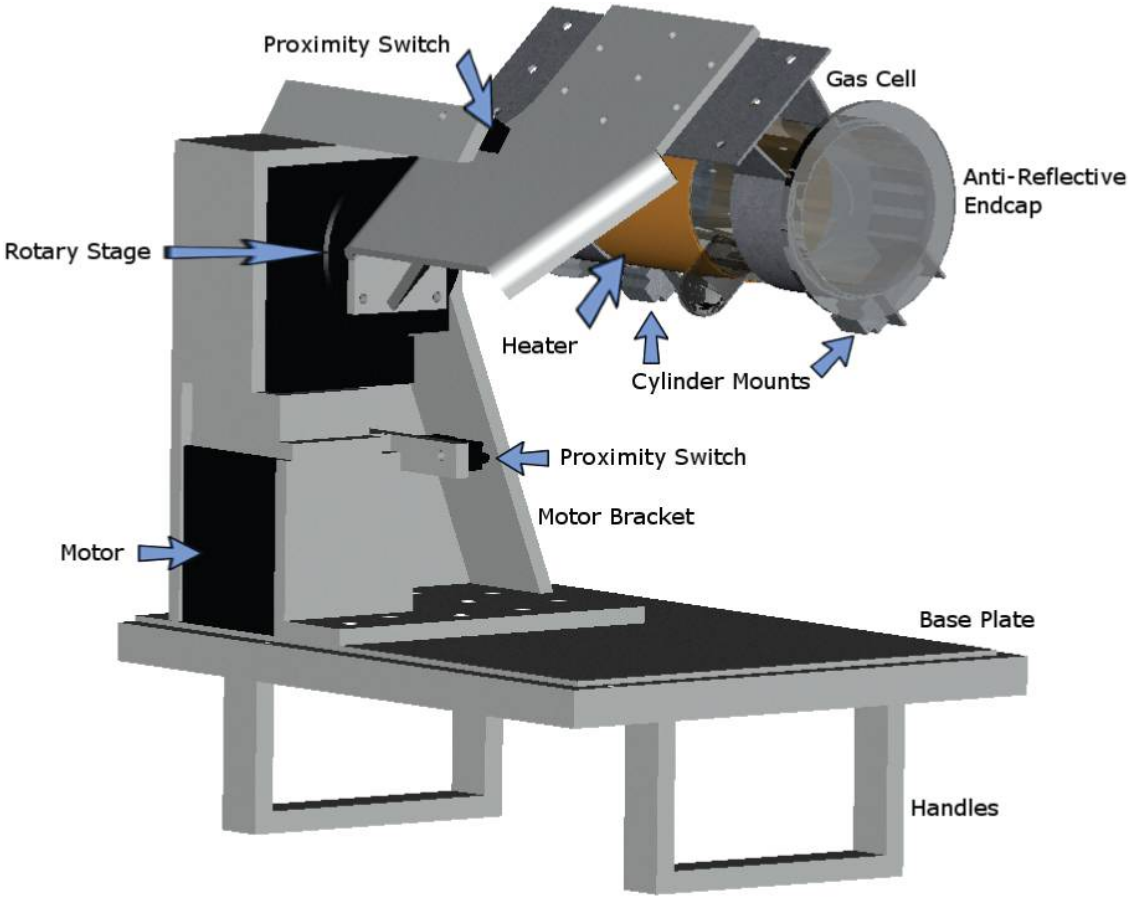

FIG. 3.—Rendering of the CAD design of the gas cell, rotary stage, and mounting mechanism. Note the heating element and the thickness of the aluminum braces (*gray*) to maintain rigidity and prevent rotation of the cell for consistent placement in the beam. Wires and bolts are omitted for visual clarity. See the electronic edition of the *PASP* for a color version of this figure.

essential design feature for ease of use and efficiency of observations, given that CSHELL mounts at the telescope Cassegrain focus. The cell sits in the converging f/38 beam prior to the beam's entrance into the spectrograph's entrance window. For this reason, the cell absorption spectrum is imprinted on the stellar light before the light goes into the spectrograph optics. The available physical space limitations for the cell ($\sim 15 \times 15 \times 18$ cm^3) placed severe design constraints on the size of the cell and the motor mechanism to move the cell in and out of the telescope beam. The length of the cell is limited on one end by the entrance window to the calibration unit and on the other end by the descending fold mirror for the calibration lamps.

The IRTF telescope dome experiences ambient temperature ranges of 276 to 284 K. In order to mitigate velocity calibration errors due to temperature changes of the cell's gas, its temperature is stabilized with a small silicon heater. For consistency, it is heated to 283 K (10°C), at the high end of dome temperatures experienced over the past year. The cell has a resistance temperature detector (RTD) sensor attached, giving temperature feedback to a temperature controller, which is expected to maintain the temperature to within ± 0.1 K. The temperature controller can be set and logged remotely to ensure stability. This should result in temperature-induced errors well below 1 m s^{-1} (Bean et al. 2010b). As a curiosity, we found that bright telluric standard stars (e.g., Sirius) heat the cell by up to ~0.5°C before the temperature controller reestablishes an equilibrium gas cell temperature (Fig. 4).

4.2. FTIR Spectra of $^{14}NH_3$, $^{13}CH_4$, and CH_3D

We have obtained laboratory measurements of the three cells' spectra at the Jet Propulsion Laboratory (JPL) using a Bruker IFS 125/HR spectrometer, for which the instrumental setup can be found elsewhere (e.g., Sung. et al. 2008, 2012, in preparation). The FTIR spectra were taken at a resolution $R \approx 700,000$ at 2.0 μm and 298 K. This resolution is much higher than CSHELL's resolution of $\sim 46,000$ and allows for very precise resolution of the individual spectral absorption features of all three gases. In order to ensure that we had complete coverage of the infrared bands we intended to use, a full scan from 1 to 5 μm wavelengths was performed. The Fourier transform spectroscopy (FTS) system at JPL is equipped with a temperature-stabilized He-neon laser and has enabled a frequency precision better than 0.0001 cm^{-1} in the scanned region, where the units of frequency are wave numbers per unit of length. The internal frequency accuracy is better than 0.01 cm^{-1}, which would correspond to a Doppler offset of 740 m s^{-1} at the K band. Because precision radial velocity measurements are always relative, extreme absolute accuracy (as opposed to precision) is not required for this experiment. If the spectra we provide need to be used for accurate frequency work, the $^{14}NH_3$ and $^{13}CH_4$ wavelengths can be refined to match the FTIR spectra to the predicted line positions from HITRAN around 3.0 μm, where all the species have abundant (and well-documented) spectral features.

We scanned the cell while the FTS was pumped down to 95 to prevent leaks of ammonia, which is known to be sticky and is notorious for leaving permanent residues on the optical surfaces. This pressure is slightly higher than the cell pressure, minimizing the risk of leaks. For the methane isotopologues, the FTS was evacuated to better than 1 mbar in pressure. For all three cases, we obtained the spectra without the cell at a pressure similar to that of each cell. In this way, the unwanted atmospheric residual features could be canceled out by dividing the cell spectra by their *no-cell* counterparts. The normalized

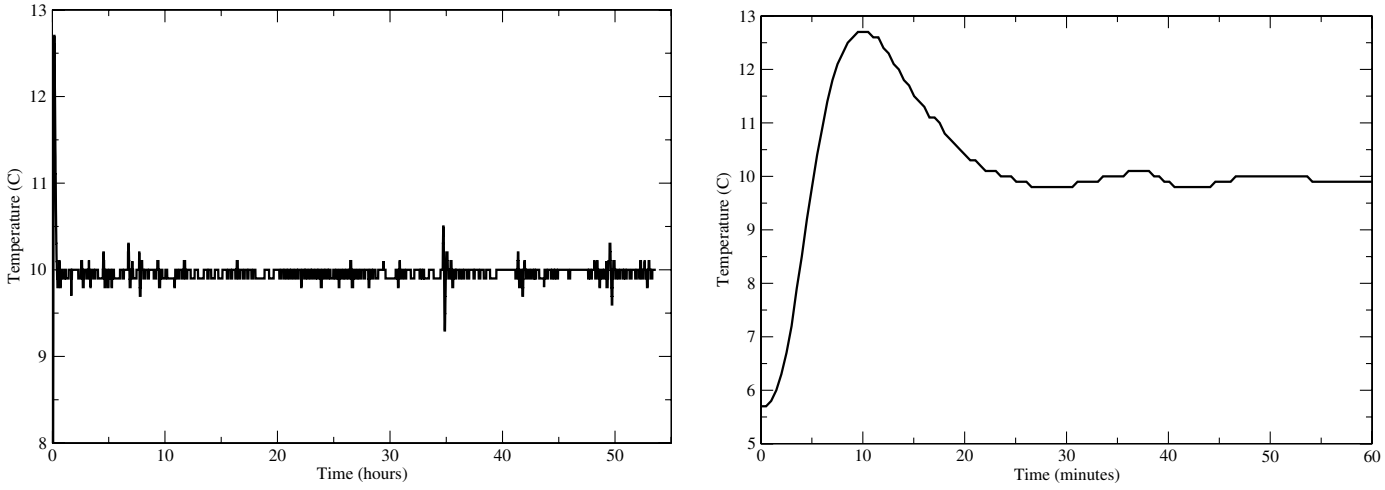

FIG. 4.—*Left*: Gas cell temperature stability as a function of hours during first light. Spikes in the temperature can be seen of up to 0.5°C and are due to observations of very bright standards heating the gas cell. *Right*: Gas cell temperature as a function of minutes during the first hour of turning the heater on. The gas cell stabilizes at the desired temperature within 1 hr.

K-band FTIR spectra of the cells are shown in Figure 5. A synthetic spectrum of a $T = 3000$ K star (~M5V) is shown on the top for comparison. The second spectrum in Figure 5 is a sample of the Earth's atmosphere absorption along the K band. Compared with the spectra of $^{13}CH_4$ (fourth row), it is easy to identify the features due to telluric methane (e.g., look for the gap at 2313 nm, which appears at 2321 nm in the $^{13}CH_4$ spectrum). Water vapor is a major contributor to the telluric absorption beyond 2400 nm. The $^{14}NH_3$ cell is in remarkable agreement with the one obtained by our synthetic spectra generator. As expected, the $^{13}CH_4$ spectrum looks very similar to the one from $^{12}CH_4$, which validates our optimization procedure. The $^{12}CH_3D$ spectrum contains a very high density of shallower lines. Even though $^{12}CH_3D$ has a higher density of lines, it is not usable for CSHELL, because at $R = 46,000$, those lines are not deep enough to be competitive against $^{14}NH_3$ or $^{13}CH_4$. Still, our laboratory-obtained spectra of $^{12}CH_3D$ can now be used to design optimal cells on other spectrographs. Even though the atmospheric contamination is less significant around 2150 nm, neither the gas cell nor the stellar spectra contain many strong absorption features around that wavelength.

Our FTIR spectra were obtained at a temperature of 298 K, whereas we are operating the gas cell on the IRTF telescope at a temperature of 283 K. Simulated spectra indicate that the difference in temperature introduced a small systematic offset of the order of 1 m s^{-1} or less. While this should not affect our relative RV measurements, the FTIR spectrum of prospective cells should be obtained at the same telescope operation temperature to guarantee that the forward modeling of the observed spectra is as accurate as possible.

4.3. *H* Band

We show the absorption spectra of our three cells in the H band (see Fig. 6). Similar to K, the H band is surrounded by very variable water vapor features from the Earth's atmosphere that should be avoided. The central part of the H band is dominated by two prominent bands of CO_2 that are known to be quite stable and have been used to reach precision radial velocities at the level of 10 m s^{-1} (Figueira et al. 2010). Both methane isotopologues show abundant lines on the redder part of the band, while ammonia has a very promising band on the bluer part. Even though the ammonia absorption is quite prominent, such a band is not listed in HITRAN 2008, so it was a surprise to find it there. Since the gases were not optimized for H-band work, the absorption lines of all three cells are too shallow to produce competitive results, compared with the K band. Testing the H band would require the construction of additional cells and was beyond the scope of our limited budget for this initial study. There are other gases and isotopologues that provide useful absorption features around 1500 nm. Some of the most promising ones have already been discussed by Mahadevan & Ge (2009) and Valdivielso et al. (2010). From our obtained spectra, a higher-pressure cell combining $^{14}NH_3$ and $^{13}CH_4$ would seem to be a good choice to cover a good fraction of the H band. Because the stellar spectra of cool dwarfs have fewer features than other IR bands (Reiners et al. 2010), and because there are other

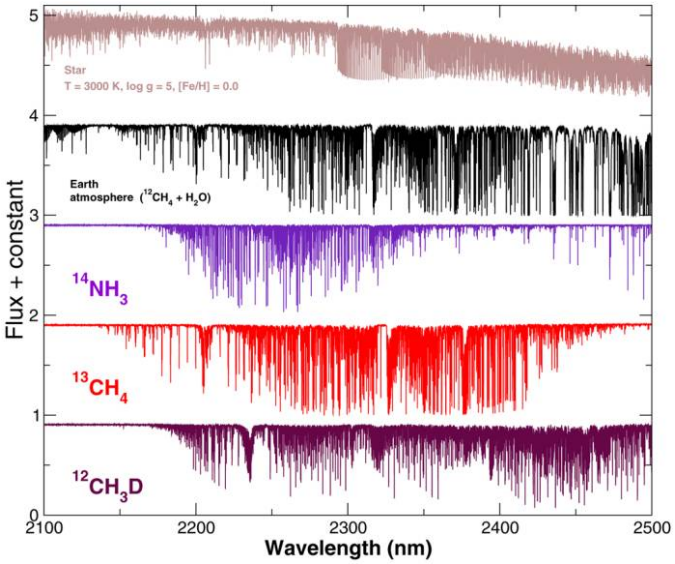

FIG. 5.—Relevant spectral features in the K band. From top to bottom: synthetic spectrum of an M5V star, absorption spectrum of the Earth's atmosphere, and laboratory-obtained spectra of our cells: $^{14}NH_3$, $^{13}CH_4$, and $^{12}CH_3D$ ($R \sim 700,000$). See the electronic edition of the *PASP* for a color version of this figure.

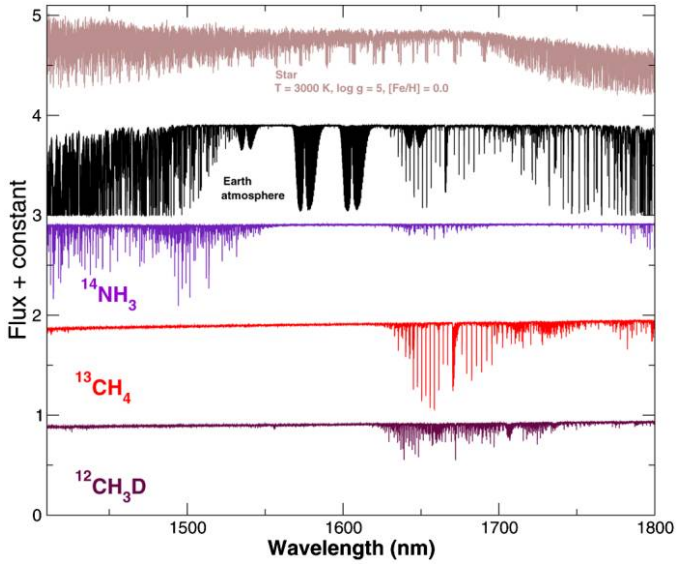

FIG. 6.—Relevant spectral features on the H band. From top to bottom: Synthetic spectrum of an M5V star, absorption spectrum of the Earth's atmosphere, and laboratory-obtained spectra of our cells: $^{14}NH_3$, $^{13}CH_4$, and $^{12}CH_3D$ ($R \sim 700,000$). See the electronic edition of the *PASP* for a color version of this figure.

studies focused on this wavelength range, we do not discuss the H band further.

4.4. First Light

The $^{13}CH_4$ cell was successfully integrated in the CSHELL spectrograph, and first light was achieved on 15 September 2010. We choose a window centered at $\lambda = 2312.5$ nm, because it is almost free of telluric features. The laboratory spectrum of the cell compared with the obtained spectrum of a telluric standard (Vega) through the cell at the telescope is shown in Figure 7. The spectra confirm the presence of the methane in the cell and a wavelength window relatively free of telluric features. The observed spectra are in excellent agreement with our expectations. We measure an effective FWHM of $\delta\lambda \sim 1.8$ pixels in the wavelength direction. The only prominent telluric line is present at pixel 120. Spectra are extracted from the raw FITS image using a custom pipeline to perform a sum of counts over the spatial direction as a function of wavelength. The exposures were taken at two node positions separated by 10″, which were then subtracted to remove the sky contribution. The raw frames were also cleaned for hot pixels, dead pixels, and cosmic-ray events. Several hundred high-S/N spectra ($S/N \sim 150$, one spectra every 30 s) of the supergiant star SV Peg (M7, K magnitude of -0.4) were also obtained in the first two nights, confirming that both the absorption-cell features and the stellar spectrum had abundant lines in the selected wavelength range (see Fig. 8).

A preliminary version of our RV extraction pipeline indicates that a precision of ~35 m s^{-1} can be obtained for each spectrum

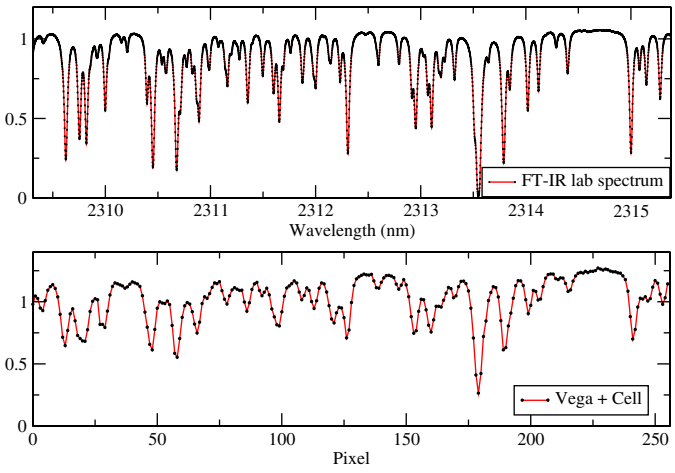

FIG. 7.—Laboratory FTIR spectrum (*top*) and observed spectrum (*bottom*) at IRTF of the $^{13}CH_4$ cell on the K-band window used for CSHELL observations. CSHELL is not cross dispersed and only covers ~6 nm at the K band. The only remarkable telluric feature in this window is at pixel 120 and corresponds to telluric methane absorption. The resolution of the FTIR spectrum is 700,000. The lines in the observed spectrum look shallower, due to the lower resolution of the spectrograph ($R = 44,000$). See the electronic edition of the *PASP* for a color version of this figure.

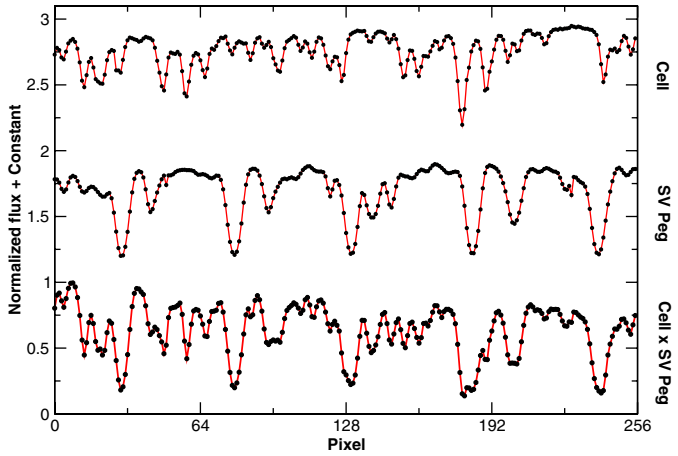

FIG. 8.—*Top*: Obtained spectrum of a telluric standard (Vega) observed through the $^{13}CH_4$ absorption cell. *Middle*: Observed spectrum of the M7 giant star SV Peg observed without the cell. *Bottom*: Observed spectrum of SV Peg through the cell. See the electronic edition of the *PASP* for a color version of this figure.

of SV Peg (see Fig. 9). Our RV determination is based on the forward-modeling technique described by Butler et al. (1996). In brief, we have developed a custom MATLAB code for our analysis. We convolve a model LSF with a model for the intrinsic spectrum of a target star, a model for the telluric spectrum of Earth's atmosphere (Wallace et al. 1996), the FTIR spectrum for the gas cell, and a fourth-order polynomial model for the continuum. The model LSF consists of a central Gaussian

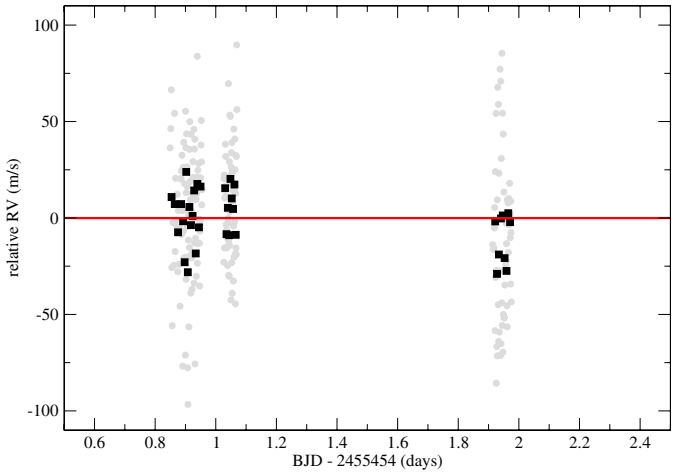

FIG. 9.—Relative radial velocity measurements of the supergiant star SV Peg ($K = -0.4$) obtained during the first two nights. Each spectrum has a formal S/N of about 150. Gray points correspond to individual observations (rms ~ 35 m s^{-1}). Black points correspond to averaged blocks of six observations. The measured rms of the averaged blocks (~14.8 m s^{-1}) is almost identical to what would be expected from Gaussian white noise ($35/\sqrt{6} = 14.2$ m s^{-1}). SV Peg is a supergiant star and, as such, should show some RV variability in timescales of a few days and may explain the ~10 m s^{-1} offset between the mean of the two nights. See the electronic edition of the *PASP* for a color version of this figure.

and N satellite Gaussians with adjustable widths, relative amplitudes, and centroids to attempt to reproduce the observed variability in the instrumental LSF. We also allow for a variable spectrograph resolution and plate scale along the length of the slit. The residuals between the model and observations are iteratively minimized over the multiple free parameters via a hybrid amoeba simplex algorithm from an initial starting set of parameters that are constrained via a coarse χ^2 minimization. We derive a deconvolved template spectrum for the target star using an iterative procedure, adding averaged residuals from our fits using the above procedure to observations taken without the gas cell. From the fit parameters, we derive the line-of-sight radial velocity to a target star from the relative wavelength shift between the model for the gas cell and the stellar template. Using standard barycentric correction routines (Stumpff 1980), we correct for barycentric motion of the observer to arrive at the final radial velocities obtained on the first two nights of observations, as shown in Figure 9. SV Peg was chosen to be very bright and with spectral features in the K band, but it is an M supergiant star and, as such, RV variability at the 10–100 $\mathrm{m\,s^{-1}}$ level is expected in timescales of a few days. Also, as happens in the optical, obtaining accurate templates is a major limitation of the absorption-cell method. To derive more reliable templates, we are now obtaining very high resolution spectra in the K band using CRIRES/VLT ($R \sim 110,000$). The long-term stability of our setup will be demonstrated in a forthcoming publication using observations on known RV-stable M dwarfs (e.g., GJ 15A and GJ 293).

5. CONCLUSIONS AND CURRENT WORK

We demonstrated a methodology to design optimal gas cells for precision RV measurements using high-resolution spectrographs. Our numerical experiments showed that with a high-resolution spectrograph covering the K band, precisions better than $5\ \mathrm{m\,s^{-1}}$ level can be achieved for late-M dwarfs ($T < 3500$ K), enabling the detection of terrestrial planets orbiting in their habitable zones. Additionally, precision RVs of earlier-type G0 to mid-K dwarfs could also be obtained, enabling planet-search programs around young active stars. We constructed two such methane isotopologue cells and presented FTIR spectra useful for future RV applications and isotopic abundance determination on solar system studies. We commissioned the $^{13}CH_4$ gas cell on CSHELL/IRTF, and provided optimal parameters for future spectrographs with the ability to operate in the K band. Even if the final $^{12}CH_3D$ cell was suboptimal for work in the K band, we found that this isotopologue of methane has an even higher density of lines. Using the obtained FTIR spectra, a cell with $^{12}CH_3D$ can also be now optimized. A similar increase in line density would be expected from a deuterated isotopologue of ammonia (e.g., $^{14}NH_2D$). Unfortunately, no comprehensive line lists exist for such species. We plan to better characterize some of these isotopologues in the future using laboratory FTIR spectroscopy and custom-made cells.

The absorption-cell technique discussed here consists of inserting the cells directly on the optical path of the starlight. Given a stabilized spectrograph (e.g., HARPS/ESO), such cells could also be used as external calibration sources by illuminating them with white light and producing a "lamplike" calibration spectrum in absorption (see Mahadevan & Ge [2009] for a more detailed discussion). However, stabilized spectrographs are more expensive to build, tend to be less versatile, and are not currently available to work in the NIR. Alternative methods to provide external wavelength calibration have been proposed (e.g., frequency comb and/or a stabilized etalon), but they will also only work on stabilized spectrographs. The absorption-cell technique remains as the only option if precision RV measurements are needed from general-purpose instruments such as NIRSPEC/Keck, CRIRES/VLT, or the planned i-Shell/IRTF.

In October 2010, we started a pilot program to obtain RV measurements on late-type young dwarfs (K and M). The targeted radial velocity precision is between 30 and $50\ \mathrm{m\ s^{-1}}$ (depending on the spectral type). An end-to-end data analysis pipeline is being developed that applies the forward-modeling technique outlined in Butler et al. (1996). Stellar spectra templates at higher resolution (using CRIRES/VLT, $R = 110,000$) are being obtained to be used in the modeling of the observed spectrum. The first results of our survey and the long-term stability of our cells will be presented in a forthcoming publication. Preliminary intranight measurements on the giant star SV Peg indicate that a precision down to $35\ \mathrm{m\ s^{-1}}$ ($\mathrm{S/N} = 150$) is within our reach. Note that we are only using 6 nm out of 300 nm available in the K band. Preliminary analysis of the most recent observing run (2011 August) confirms that the $^{13}CH_4$ gas cell pressure and operation remains nominal after nearly one year of operation on the telescope at the summit of Mauna Kea, Hawaii. Given the better nominal performance of methane isotopologues compared with $^{14}NH_3$, and assuming that the photon noise is a significant term in the final error budget, a $^{13}CH_4$ (or $^{12}CH_3D$) cell installed on a CRIRES-like spectrograph and a setup similar to the one used by Bean et al. (2010a), should lead to a 30–40% improvement in the overall Doppler accuracy (3–4 $\mathrm{m\ s^{-1}}$ precision compared with the current $6\ \mathrm{m\ s^{-1}}$ long-term accuracy demonstrated on Barnard's star and Proxima Centauri). Bean et al. (2010a) discussed that the likely limiting factor of the ammonia CRIRES program was contamination by shallow telluric features, both on the observations and during the stellar template reconstruction. While this is a likely source of systematic uncertainty, our numerical simulations indicate that the ammonia cell's contribution to the error budget has almost the same magnitude as the reported rms on RV-stable stars. We therefore conclude that even though telluric contamination is definitely a source of uncertainty, using a methane cell on CRIRES should lead to a significant increase in precision. Given that enough space is left between the telescope and the spectrograph ($\sim$10 cm), such cells can be installed

at little cost in upgraded versions of the available NIR instruments (e.g., NIRSPEC at Keck and CRIRES/VLT) and planned instruments with *K*-band capabilities (e.g., i-Shell at NASA/IRTF).

Both G. Anglada-Escudé and P. Plavchan contributed equally to this work. G. A. would like to acknowledge the Carnegie Postdoctoral Fellowship Program and the support provided by the NASA Astrobiology Institute grant NNA09DA81A. Peter Plavchan would like acknowledge Wes Traub and Stephen Unwin for funding provided by the Jet Propulsion Laboratory's (JPL's) Center for Exoplanet Science and NASA Exoplanet Science Institute. K. Sung acknowledges the Planetary Atmospheric Research Program to support the laboratory spectroscopic calibrations. Part of the research at the JPL and California Institute of Technology was performed under contracts with National Aeronautics and Space Administration. We thank Anu Dudhia for making the Reference Forward Model code available to us and for his assistance with adapting it for gas cell spectral calculations. The stellar synthetic spectra were graciously provided by Peter Hauschildt (University of Hamburg) and the PHOENIX group. We also thank Linda Brown from JPL's Laboratory Studies and Modeling group and Pin Chen from the Planetary Chemistry and Astrobiology group for their advice and support using the Fourier-transformed infrared spectrometer. We would like to thank Paul Butler (Carnegie Institution of Washington) and Gilian Nave (NIST) for their advice in gas optimization parameters and molecular spectroscopy in general. We would like to thank Stephen Kane (NExScI), Kaspar von Braun (NExScI), and Steve Osterman (University of Colorado) for their valuable discussions. We also thank John Rayner, Morgan Bonnet, George Koenig, and Alan Tokunaga from IfA, Hawaii, for their support during the CSHELL/IRTF cell design review, integration, and commissioning. We thank Rick Gerhart (California Institute of Technology), Scot Howell (Mindrum Precision), and Thurston Levy (Glass Instruments, Inc.) for their work in helping construct and fill the gas cells, as well as Joeff Zolkower (California Institute of Technology) for mechanical engineering advise.

REFERENCES

Bailey, J., White, R., & Blake, C., et al. 2012, ApJ, accepted
Bean, J. L., Seifahrt, A., & Hartman, H., et al. 2010a, ApJ, 711, L19
———. 2010b, ApJ, 713, 410
Boudon, V., Champion, J., & Gabard, T., et al. 2009, Europhys. News., 40, 17
Butler, R. P., Marcy, G. W., & Williams, E., et al. 1996, PASP, 108, 500
Charbonneau, D., Berta, Z. K., & Irwin, J., et al. 2009, Nature, 462, 891
Crane, J. D., Shectman, S. A., & Butler, R. P., et al. 2010, Proc. SPIE, 7735, ??
Endl, M., Cochran, W. D., Kürster, M., & PaulsonD. B., et al. 2006, ApJ, 649, 436
Figueira, P., Pepe, F., & Melo, C. H. F., et al. 2010, A&A, 511, A55
Ge, J., Erskine, D. J., & Rushford, M. 2002, PASP, 114, 1016
Gillon, M., Pont, F., & Demory, B.-O., et al. 2007, A&A, 472, L13
Greene, T. P., Tokunaga, A. T., Toomey, D. W., & Carr, J. B. 1993, Proc. SPIE, 1946, 313
Hauschildt, P. H., Allard, F., & Baron, E. 1999, ApJ, 512, 377
Howard, A. W., Marcy, G. W., & Johnson, J. A., et al. 2010, Science, 330, 653
Huang, X., Schwenke, D., & Lee, T. 2008, J. Chem. Phys., 129, 214304
Johnson, J. A., Butler, R. P., & Marcy, G. W., et al. 2007, ApJ, 670, 833
Kaeufl, H.-U., Ballester, P., & Biereichel, P., et al. 2004, Proc. SPIE, 5492, 1218
Mahadevan, S., & Ge, J. 2009, ApJ, 692, 1590
Mayor, M., Bonfils, X., & Forveille, T., et al. 2009, A&A, 507, 487
McLean, I. S., Becklin, E. E., & Bendiksen, , et al. 1998, Proc. SPIE, 3354, 566
Reiners, A., Bean, J. L., Huber, K. F., Dreizler, S., Seifahrt, A., & Czesla, S. 2010, ApJ, 710, 432
Rivera, E. J., Laughlin, G., Butler, R. P., Vogt, S. S., Haghighipour, N., & Meschiari, S. 2010, ApJ, 719, 890
Rothman, L., Gordon, I., & Barbe, A., et al. 2009, JQSRT, 110, 533
Shen, N.-C., Wu, Y.-X., Sun, Y.-M., Li, C.-Y., Zhang, X.-B., & Wang, C. 1981, in Precision Measurement and Fundamental Constants, ed. B. N. Taylor, & W. D. Phillips (Washington: NBS), 77
Stumpff, P. 1980, A&AS, 41, 1
Sung., K., Brown, L. R., Toth, R. A., & Crawford, T. J. 2008 Canadian J. Phys., 87, 469
Tokunaga, A. T., Toomey, D. W., Carr, J., Hall, D. N. B, & Epps, H. W. 1990, Proc. SPIE, 1235, 131
Urban, Š., Tu, N., Narahari RaoK., & Guelachvili, G. 1989, J. Mol. Spectrosc., 133, 312
Valdivielso, L., Esparza, P., Martín, E. L., Maukonen, D., & Peale, R. E. 2010, ApJ, 715, 1366
Vogt, S. S., Butler, R. P., Rivera, E. J., Haghighipour, N., Henry, G. W., & Williamson, M. H. 2010, ApJ, 723, 954
Wallace, L., Livingston, W., Hinkle, K., & Bernath, P. 1996, ApJS, 106, 165
Yurchenko, S. N., Zheng, J., Lin, H., Jensen, P., & Thiel, W. 2005, J. Chem. Phys., 123, 134308
Zechmeister, M., Kürster, M., & Endl, M. 2009, A&A, 505, 859